Cilt 11, Sayı 2, Sayfa 76-81, 2022 Volume 11, Issue 2, Page 76-81, 2022

Araştırma Makalesi https://doi.org/10.46810/tdfd.1106743 Research Article

Türk Doğa ve Fen Dergisi
Turkish Journal of Nature and Science
www.dergipark.gov.tr/tdfd

Investigation of Microstructural, Mechanical and Corrosion Properties of Cu-10Sn Bronze Parts Produced by Selective Laser Melting

Mustafa Naci TOP [1], Semih ÖZBEY [2], Batuhan SORUŞBAY[2], H.Özkan GÜLSOY [2*]

[1] Marmara University, Institute Graduate Studies Pure and Applied Sciences, 34722, Göztepe-Istanbul, Türkiye
[2] Marmara University, Technology Faculty, Metalurgy and Materials Eng., 34722, Göztepe-Istanbul, Türkiye

Mustafa Naci TOP ORCID No: 0000-0002-8947-6245
Semih ÖZBEY ORCID No: 0000-0001-5582-9973
Batuhan SORUŞBAY ORCID No: 0000-0001-8108-1399
H.Özkan GÜLSOY ORCID No: 0000-0001-5366-5741

**Corresponding author: ogulsoy@marmara.edu.tr*

(Received: 21.04.2022, Accepted: 23.05.2022, Online Publication: 29.06.2022)

Keywords
Selective Laser Melting, Cu-Sn alloy, Microstructure, Mechanical properties, Corrosion resistance

Abstract: In this study, the production of full-density Cu-10Sn bronze parts by selective laser melting (SLM) technique and the examination of microstructural, mechanical and corrosion properties were carried out. Cu-10Sn pre-alloyed powders produced by gas atomization technique were shaped using SLM technique within selected parameters and then microstructural properties were determined. Depending on the microstructural properties, the mechanical and corrosion behaviors were determined. The obtained results were compared with similar bronze materials produced by conventional methods. Different characterization techniques were used for microstructural characterization. The microstructure of the Cu-10Sn alloy was observed to consist of dendritic primary α and δ-$Cu_{41}Sn_{11}$ phases. According to the mechanical test results of the samples produced at densities of 8.75 g cm^{-3} at room temperature, the yield strength was measured as 420 MPa, the tensile strength was 578 MPa, the elongation was 32 % and the hardness value was 160.3 $HV_{0.2}$. For the electrochemical experiments, the corrosion rate of the samples was found to be 4.38 mpy. As a result of the productions and experiments, it was determined that the samples produced by the SLM method provide very good mechanical and corrosion properties compared to the literature.

Seçici Lazer Ergitme Tekniği İle Üretilmiş Cu-10Sn Bronz Parçaların Mikroyapısal, Mekanik ve Korozyon Özelliklerinin İncelenmesi

Anahtar Kelimeler
Seçici Lazer Ergitme, Cu-Sn alaşımı, Mikroyapı, Mekanik özellikler, Korozyon direnci

Öz: Bu çalışmada, tam yoğunluklu Cu-10Sn bronz parçaların seçici lazer ergitme (SLM) tekniği ile üretilmesi, mikroyapısal, mekanik ve korozyon özelliklerinin incelenmesi gerçekleştirilmiştir. Gaz atomizasyon tekniği ile üretilmiş Cu-10Sn ön-alaşımlı tozlar, seçilen parametreler dahilinde SLM tekniği kullanılarak şekillendirilmiş ve sonrasında mikroyapısal özellikleri belirlenmiştir. Mikroyapısal özelliklere bağlı olarak mekanik ve korozyon davranışlarının belirlenmesi gerçekleştirilmiştir. Elde edilen sonuçlar geleneksel metotlar ile üretilmiş benzer bronz malzemeler ile karşılaştırılmıştır. Mikroyapısal karakterizasyon için farklı inceleme teknikleri kullanılmıştır. Cu-10Sn alaşımının mikroyapısının dendritik birincil α ve δ-$Cu_{41}Sn_{11}$ fazlarından oluştuğu görülmüştür. 8,75 g cm^{-3} yoğunluklarda üretilen numunelerin oda sıcaklığında gerçekleştirilen mekanik deney sonuçlarına göre, akma mukavemeti 420 MPa, çekme mukavemeti 578 MPa, % uzama değeri 32 ve sertlik değeri 160,3 $HV_{0.2}$ olarak ölçülmüştür. Gerçekleştirilen elektrokimyasal deneylere göre numunelerin korozyon hızının 4,38 mpy değerlerinde olduğu görülmüştür. Gerçekleştirilen üretimler ve deneyler sonucunda SLM yöntemiyle üretilen numunelerin literatüre kıyasla oldukça iyi mekanik ve korozyon özellikleri gösterdiği belirlenmiştir.

1. INTRODUCTION

Cu-Sn alloys are traditionally used in the manufacture of musical instruments, artistic objects and engineering applications. In addition, Cu-Sn alloys are frequently used in electronics, aerospace and defense applications due to their high strength, superior wear resistance, high corrosion resistance, good weldability, high thermal and electrical properties. Other important application areas are heat exchangers, high precision springs and bearings, electronic fasteners and plastic deformation sensitive applications [1–5].

Owing to superior resistance to corrosion in seawater, Cu–Sn alloys have also been adopted in the marine industry as propulsion devices [2, 3]. In general, bronze with low level of Sn (less than 5 wt.%) intended for plastic working is widely used in electrical and electronic industries such as sensitive elements of pressure gauges and electrical connectors as well as high-precision springs. With the increase of Sn content, mechanical properties can be strengthened. When the Sn content exceeds 10%, alloy exhibit excellent mechanical properties, wear resistance and corrosion resistance [6]. Post-machining processes, such as forging, rolling, drawing, and/or bending, are essential for manufacturing precise and complex mechanical parts of alloys in desired shapes. However, the formation of the brittle δ phase in the high tin bronze alloy causes difficulties during plastic deformation. Therefore, the Cu–Sn alloys with tin content above 10%, termed high-tin bronze, is fabricated primarily by casting [3, 7]. In traditional casting technology, decrease in mechanical properties due to large grain size, shrinkage cavity and pores, the low solubility in the solid solution phase and serious grain boundary segregation, and the inability to produce complex parts in conventional powder metallurgy limits the production of Cu-Sn alloys. Compared with traditional casting technology, the novel-developed additive manufacturing (AM) technology can fabricate parts with complex structures with improved microstructure and mechanical properties, avoiding the defects introduced by casting technology [4]. Selective laser melting (SLM), a laser powder-bed fusion process, is one of the frontrunners in the accepted AM technologies. SLM, where production is done layer by layer, offers the ability to produce complex structural parts that have unchallenged design freedom, maximum material savings, high dimensional accuracy, and excellent surface finish. Using SLM, many engineering materials, including steels, Ni-alloys, Co-alloys, Ti-alloys, Al-alloys, high-entropy alloys, etc., have been successfully fabricated with properties comparable to those achieved in conventional processing methods [1, 8]. SLM also offers the possibility to produce metastable phases and microstructures due to its small size (µm size volume) melt pool and corresponding high cooling rates [9, 10].

Due to the layer-by-layer production of parts in the SLM technique, parts undergo complex thermal cycles. Rapid cooling rates with SLM cause nonequilibrium solidification, increase in solid solubility and finer grain size [11]. Moreover, the high thermal gradient and local inhomogeneous heating-cooling cycles result in a heterogeneous microstructure with high dislocation density and cellular structure [12, 13]. The unique microstructures developed during the SLM process allow the development of high-performance materials compared to their counterparts produced by conventional methods [11, 14, 15].

Due to copper's high thermal conductivity, the melt area experiences rapid heat dissipation and high local thermal gradients, resulting in delamination, layer curling, and part failure [16]. In addition, it has been determined that the production of copper alloys is relatively easy compared to pure copper [2, 11]. While alloying elements added to copper significantly reduce its conductivity, it widens the solidification range and lowers the Gibbs melting energy. As a result, sufficient time is provided for the molten metal to spread evenly over the previous layer to achieve good bonding with low porosity [16, 17]. With all this information, it seems possible to produce Cu-Sn bronze parts with the AM technique and to use them especially for marine applications.

In this study, Cu-10Sn bronze samples were produced by SLM technique to investigate the production of Cu-based alloys by additive manufacturing. The densities of the produced samples were measured according to the Archimedes principle. The microstructure, mechanical properties and corrosion behavior of the samples were examined and the findings were discussed in consideration of the literature. Experimental studies include scanning electron microscopy (SEM) and X-ray diffraction (XRD) analysis for initial powder morphology, microstructural evolution and analysis of fractured surfaces; Tensile tests and hardness measurements were performed to determine the mechanical properties, and electrochemical measurements were performed to determine the corrosion behavior.

2. MATERIALS AND METHODS

While preparing the samples, PM-BR101P (Powmet, Italy) spherical bronze powders (Cu-10Sn) produced by gas atomization, especially developed for laser melting applications, were used. Gas atomized powders are generally spherical in shape and exhibit high purity, fluidity and packaging properties [18, 19]. Powder morphology was visualized with FEI-Srion brand SEM and images are given in Figure 1. It is observed from that the particle shape of Cu-10Sn pre-alloyed powders is in spherical shape and the median particle size of the powders is suitable for using in AM applications. The powder surfaces are quite smooth and there is no satelliteing. Also, Malvern Mastersizer device was used to determine the particle size distribution of the powders. The physical properties of the powders are given in Table 1. The average particle size of the powders was found to be 50 µm. Phase analysis of the powders was performed on Rigaku brand D/MAX RINT 2200 (Japan) model XRD device.

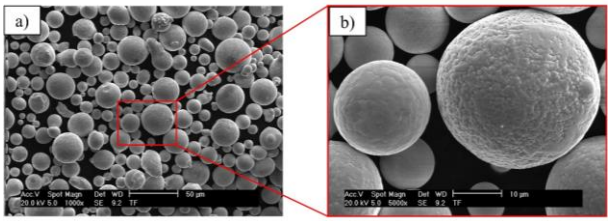

Figure 1. SEM images of Cu-10Sn powder: a) 1000 magnification, b) 5000 magnification.

Table 1. Physical properties of Cu-10Sn powders.

Physical Properties		
Density, g cm^{-3}	8.77	
Apparent density, g cm^{-3}	3.90	
Tapped density, g cm^{-3}	4.20	
Particle Size Distribution, µm	D_{10}	16
	D_{50}	25
	D_{90}	38

Two types of samples, whose images are given in Figure 2, to be used in tensile test and metallographic examinations, were produced under nitrogen atmosphere with SISMA-MYSINT100 PM (Italy) SLM device equipped with Yb-YAG, and the process parameters are given in Table 2. The energy density was calculated using Equation 1. During the production, the chess (5mmx5mm) scanning strategy was used as laser strategy.

$$E = \frac{P}{v * h * t} \qquad (1)$$

where the energy density E (J mm^{-2}) is a measure of average applied energy per unit volume of material, P is laser power (in W), v is laser scan speed (in mm s^{-1}), h is hatch spacing (in mm) and t is layer thickness (in mm) [8]. The samples were produced on a 10 cm diameter table, four bars of 10 mm diameter, 25 mm high for metallographic examinations, and two non-standard 70 mm length, 25 mm high bars to be used in the tensile test. The tensile test specimens were shaped by slicing into 2 mm thick pieces using a precision cutting machine. After grinding and polishing, samples surface roughness was made suitable for tensile testing. XRD analyzes were carried out on the building and scanning directions and the phases formed in different directions were analyzed. The samples to be used in metallographic examinations were electrolytically etched in a solution containing 50% HF and 50% distilled water for 5-10 s after the grinding and polishing. The samples were also examined in both directions at high magnifications using SEM. In the density measurements made using Archimedes principle, the average densities (at least 5 samples) were measured as 8.75 g cm^{-3} (relative densities of 99.5%).

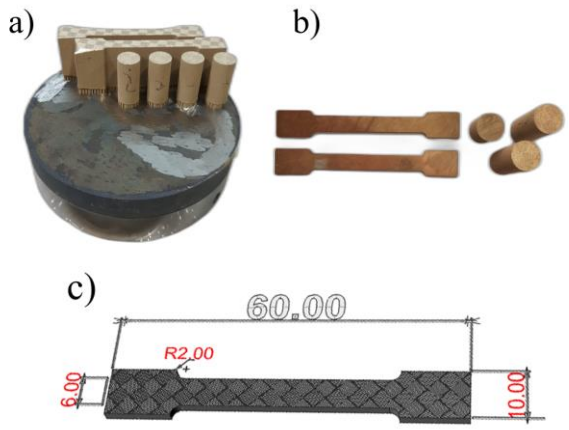

Figure 2. a) Sample images after SLM production, b) prepared samples for tensile test and metallographic investigation c) sample measurements prepared for the tensile test.

Table 2. SLM production parameters.

Laser Power W	Scan Speed mm s^{-1}	Hatch Spacing µm	Layer Thickness µm	Energy Density J mm^{-3}
110	1200	60	20	76

Microhardness measurements were made with FUTURE-TECH brand FM-310E (Japan) model microhardness device in both directions. Tensile tests were carried out on 10 specimens at a tensile speed of 25.4 mm/min with a Zwick-Z250 model device at room temperature. Tests were conducted as per the crosshead speed control method defined by ASTM E-8 standard. The fracture surfaces of the specimens that broke as a result of the tensile test were examined by SEM. The corrosion behavior of the samples was investigated in a standard 3-electrode system using a GAMR Interface 1000 (UK) potentiometer device in a seawater medium containing 3.5% NaCl. Saturated calomel electrode (SCE) was used as reference electrode and graphite electrode as counter electrode. The reliability of the experimental results was increased by repeating the mechanical tests on 5 different samples and the corrosion tests on 3 different samples.

3. RESULTS AND DISCUSSION

XRD analyzes of the powders and both building and scanning direction of the samples produced by the SLM method are given in Figure 3. When the XRD analyzes are examined, it is seen that the XRD results of the phases in the scanning direction and the powders are similar. In the both directions, the structure consists of α-Cu(Sn) and δ-$Cu_{41}Sn_{11}$ phases, while the construction direction consists of only the α-Cu(Sn) phase. The δ-$Cu_{41}Sn_{11}$ phase is formed as a result of rapid cooling in the scanning direction. [20].

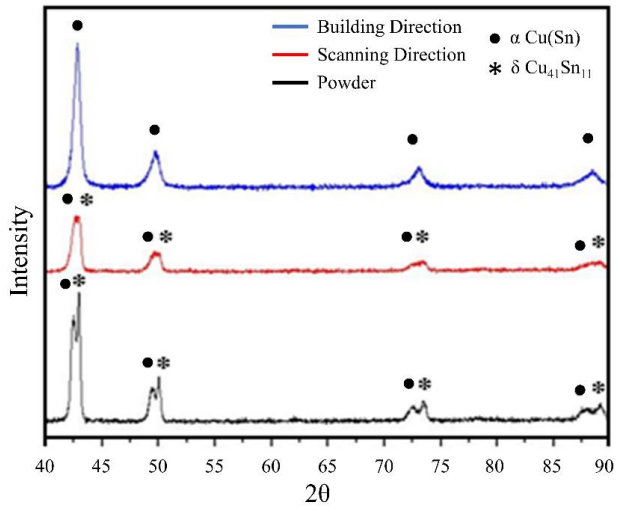

Figure 3. XRD analysis of the powders, and produced samples in the building and scanning direction.

In the SEM examinations carried out to determine the microstructures of the samples in the direction of building, it was determined that the rapid and local melting and cooling provided by the SLM technique causes very fine microstructures and very small porosities at the grain boundaries. SEM images taken from the building direction are given in Figure 4. In the building direction microstructure, especially the melting pool regions are visible and there are irregular grain boundaries between each melting pool.

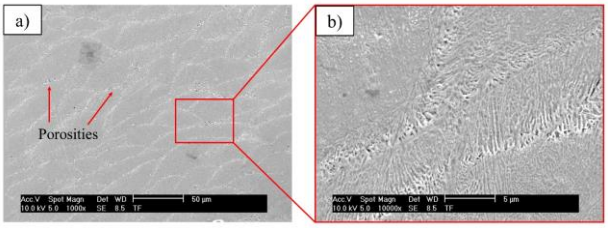

Figure 4. SEM images of the sample in the building direction: a) 1000 magnification, b) 10000 magnification.

As can be seen from high magnification SEM images, it is known that such cellular structures are due to rapid cooling and eutectic solidification. In the SEM examinations made in the scanning direction, it is seen that the δ-$Cu_{41}Sn_{11}$ phases are distributed in the microstructure, and the SEM images are given in Figure 5.

SEM image of the scanning direction given in Figure 6, it is seen that the microstructure consists of α + δ eutectoic (light color) and dendritic α (dark color) phases. In particular, the existence of very fine cellular structures consisting of α + δ phases has been observed. SEM investigations of building and scanning are in agreement with XRD analysis results.

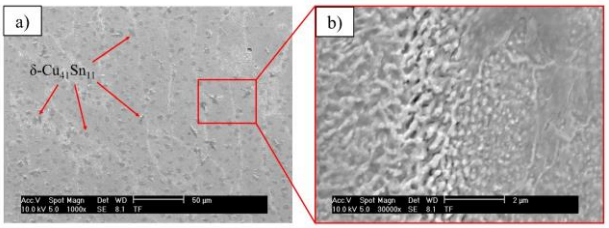

Figure 5. SEM images of the sample in the scanning direction: a) 1000 magnification, b) 30000 magnification.

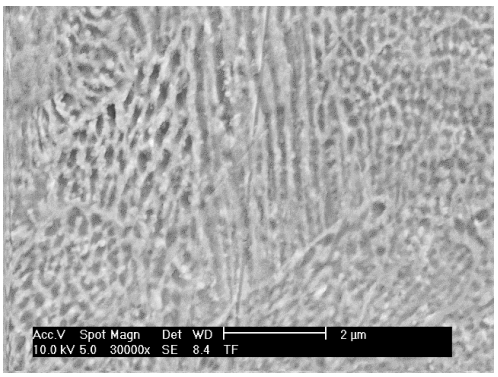

Figure 6. SEM image of the sample in the scanning direction: 30000 magnification.

As a result of the hardness measurements carried out in both directions, the highest and lowest hardness values in the building direction were 158.6 $HV_{0.2}$ and 150.6 $HV_{0.2}$; in the scanning direction, it was measured as 166.2 $HV_{0.2}$ and 161.7 $HV_{0.2}$. Although the hardness values are close to each other, the difference is due to the high hardness of the δ-$Cu_{41}Sn_{11}$ phases formed in the scanning direction [3].

The stress-strain graph obtained from tensile test is given in Figure 7, and it was observed that the sample showed an excellent combination of high strength (yield strength ~452 MPa, tensile strength ~578MPa) and ductility (32%). Compared to the Cu-10Sn alloys produced by the SLM technique in the literature, very high values were obtained. [2, 8, 21, 22]. Comparison of SLM production parameters is given in Table 3.

Table 3. Literature comparison of SLM production parameters.

Alloy	Laser Power W	Scan speed mm s^{-1}	Hatch Spacing µm	Layer Thickness µm	Energy Density J mm^{-3}	Yield and Tensile Strength MPa	Reference
Cu-10Sn	271	210	90	90	~159	220 / 420	[2]
Cu-13Sn	350	750	120	30	130	~404 / ~635	[8]
Cu-10Sn	Variable	Variable	120	30	-	- / ~550	[21]
Cu-10Sn	95	~377, ~360, ~344	60	20	210, 220, 230	~386 / ~469	[22]
Cu-10Sn	110	1200	60	20	76	~452 / ~578	Current Study
Cu-10Sn (Casting)	--	--	--	--	--	152 / 310	[23]

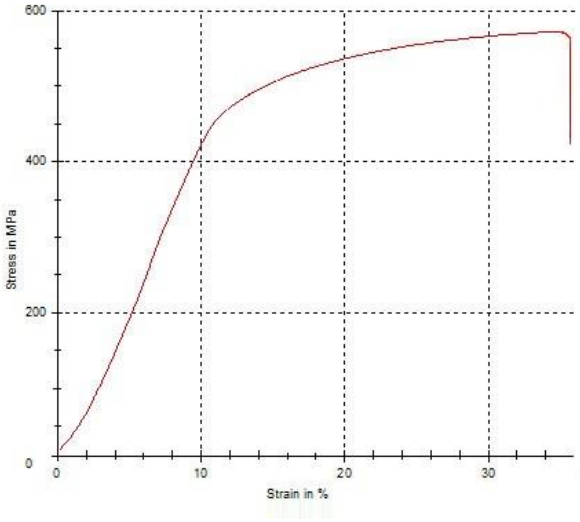

Figure 1. Stress-strain graph.

In order to interpret the fracture mechanisms of the samples as a result of the tensile tests, the fracture surfaces were examined by SEM and the images are given in Figure 8. As seen in Figure 8.b, there are dimples on the fracture surface, which are the biggest indication of ductile fracture. The large number of dimples in small size means that more surface energy is produced during fracture and therefore the strength of the material is higher. In addition, the size of the dimples is dependent on the size of the subgrains. [24]. The macropores in Figure 8.a, on the other hand, are thought to be formed as a result of ruptures especially from the edges of the melting pool.

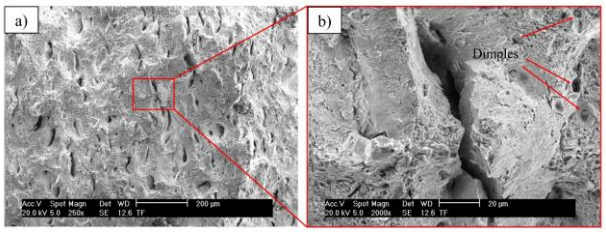

Figure 2. SEM images of the fracture surface: a) 250 magnification, b) 2000 magnification.

In Figure 9, decreasing in current density with the potential increasing has indicated that the protective layer has initiated to stably form on the sample surface. The formation of protective layer above 100mV is completely stable form and it remains with the potential increasing. Thus, it is known that the passive layer occurs on the material surface in the Tafel curve, the current density does not change with increasing potential. The data obtained by the Tafel method are given in Table 4. The corrosion rate was found to occur at 4,388 miles (1 mil=0.001 inch) per year.

Existing two and more phases in surface have sensitivity to galvanic corrosion in a corrosive media [25]. The full-density Cu-10Sn bronze parts produced by selective laser melting (SLM) technique has consist of primary α and δ-$Cu_{41}Sn_{11}$ phases. Phase distributions in the microstructure of Cu-10Sn bronze significantly affect the local corrosion development. Since primary δ-$Cu_{41}Sn_{11}$ phases higher corrosion resistance than primary α, primary δ-$Cu_{41}Sn_{11}$ phase acts as a cathode; on the other hand, primary α acts as anode [26]. Thus, the alpha phase, which is the anodic part, is significantly corroded. This has been emphasized in a previous similar study [27].

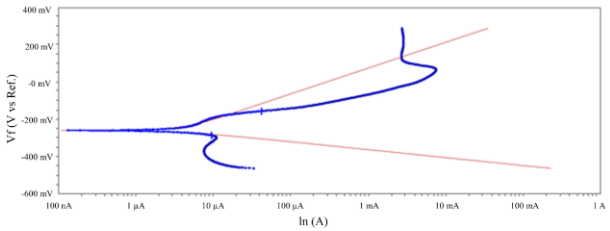

Figure 3. Tafel curve obtained from the corrosion test.

Table 4. Data obtained from the corrosion test.

Beta A	138,0e-3 V/decade
Beta C	42.,50e-3 V/decade
I_{corr}	3,860 uA
E_{corr}	-261,0 mV
Corrosion rate	4,388 mpy

4. CONCLUSION

Cu-10Sn bronze samples with almost full density (99.5%) were produced by SLM technique and their microstructure, mechanical and corrosion properties were examined and compared with other studies in the literature. As a result of XRD analysis, it was determined that α-Cu(Sn) and δ-$Cu_{41}Sn_{11}$ phases were formed in the scanning direction and α-Cu(Sn) phases in the building direction. As a result of the tensile, hardness and corrosion tests, the parts produced with SLM technique showed superior mechanical (yield strength 420 MPa, tensile strength 578 MPa, % elongation 32 and hardness value 160.3 $HV_{0.2}$) and corrosion properties (Corrosion Rate: 4.388 mpy). These findings prove that the complex shape and high strength Cu-10Sn bronze alloy can be produced effectively by SLM technique.

Acknowledgement

This study (Project no: FEN-C-YLP-130219-0042) was supported by Marmara University.

REFERENCES

[1] Li X, Ivas T, Spierings AB, Wegener K. Phase and microstructure formation in rapidly solidified Cu-Sn and Cu-Sn-Ti alloys. J Alloys Compd 2018;735: 1374–1382.

[2] Scudino S, Unterdörfer C, Prashanth KG, Attar H, Ellendt N, Unhlenwinkel V, et al. Additive manufacturing of Cu–10Sn bronze. Mater Lett 2015; 156:202–204.

[3] So S-M, Kim K-Y, Lee S-J, Yu Y-J, Lim H-A, Oh M-S. Effects of Sn content and hot deformation on microstructure and mechanical properties of binary high Sn content Cu–Sn alloys. Mater Sci Eng A 2020;796.

[4] Yang P, Guo X, He D, Shao W, Tan Z, Fu H, et al. Microstructure Twinning and Mechanical Properties of Laser Melted Cu-10Sn Alloy for High Strength

and Plasticity. Journal of Materials Engineering and Performance. 2022;31: 2624-2632.
[5] Mao Z, Zhang D, Wei P, Zhang K. Manufacturing Feasibility and Forming Properties of Cu-4Sn in Selective Laser Melting. Materials 2017; 10: 333.
[6] Mao Z, Zhang DZ, Jiang J, Fu G, Zhang P. Processing optimization, mechanical properties and microstructural evolution during selective laser melting of Cu-15Sn high-tin bronze. Mater Sci Eng A 2018; 721: 125–134.
[7] Park JS, Park CW, Lee KJ. Implication of peritectic composition in historical high-tin bronze metallurgy. Materials Characterization 2009; 60(11): 1268–1275.
[8] Karthik GM, Sathiyamoorthi P, Zargaran A, Park JM, Asghari-Rad P, Son S, et al. Novel precipitation and enhanced tensile properties in selective laser melted Cu-Sn alloy. Materialia 2020; 13: 100861.
[9] Prashanth KG, Scudino S, Klauss HJ, Surreddi K.B., Löber L, Wang Z, et al. Microstructure and mechanical properties of Al–12Si produced by selective laser melting: Effect of heat treatment. Materials Science and Engineering: A. 2014; 590: 153–160.
[10] Ma P, Prashanth K, Scudino S, Jia Y, Wang H, Zou C, et al. Influence of Annealing on Mechanical Properties of Al-20Si Processed by Selective Laser Melting. Metals 2014; 4(1): 28–36.
[11] Wang J, Zhou XL, Li J, Brochu M, Zhao Y. Microstructures and properties of SLM-manufactured Cu-15Ni-8Sn alloy. Additive Manufacturing. 2019; 31: 100921.
[12] Liu L, Ding Q, Zhong Y, Zou J, Wu J, Chiu Y, et al. Dislocation network in additive manufactured steel breaks strength–ductility trade-off. Materials Today 2018; 21: 354–361.
[13] DebRoy T, Wei HL, Zuback JS, Mukherjee T, Elmer J.W, Milewski J.O, et al. Additive manufacturing of metallic components – Process, structure and properties. Progress in Materials Science. 2018; 92: 112–224.
[14] Uchida S, Kimura T, Nakamoto T, Ozaki T, Miki T, Takemura M, et al. Microstructures and electrical and mechanical properties of Cu-Cr alloys fabricated by selective laser melting. Mater Des 2019; 175: 107815.
[15] Ventura AP, Marvel CJ, Pawlikowski G, Bayes M, Watanabe M, Vinci R, et al. The Effect of Aging on the Microstructure of Selective Laser Melted Cu-Ni-Si. Metallurgical and Materials Transaction A. 2017; 48(12): 6070–6082.
[16] Tran TQ, Chinnappan A, Lee JKY, Loc NH, Tran LT, Wang G, et al. 3D Printing of Highly Pure Copper. Metals 2019; 9: 756.
[17] Tiberto D, Klotz UE, Held F, Wolf G. Additive manufacturing of copper alloys: influence of process parameters and alloying elements. Materials Science and Technology. 2019; 35: 969–977.
[18] Irrinki H, Jangam JSD, Pasebani S, Badwe S, Stitzel J, et al. Investigation of 17-4 PH Stainless Steel Fabricated by Laser- Powder Bed Fusion. International Conference on Innovative Engineering Applications, CIEA 2018. Sivas.
[19] Irrinki H, Nath SD, Alhofors M, et al. Microstructures, properties, and applications of laser sintered 17-4PH stainless steel. J Am Ceram Soc 2019; 102: 5679–5690.
[20] Ludwig A, Grasser M, Schillinger W. Experimental Investigation on the Ternary Phase Diagram Cu–Sn–P. World of Metallurgy. 2012; 65: 117-125.
[21] Gu R, Yao X, Wang D, Hang H, Yan M, Wong KS. Selective Laser Melting of Cu–10Sn–0.4P: Processing, Microstructure, Properties, and Brief Comparison with Additively Manufactured Cu–10Sn. Advanced Engineering Materials. 2022; 24(2): 2100716.
[22] Deng C, Kang J, Feng T, Wang X, Wu P. Study on the Selective Laser Melting of CuSn10 Powder. Materials 2018; 11(4): 614.
[23] B05 Committee. Specification for Copper Alloy Continuous Castings. ASTM International. DOI: 10.1520/B0505_B0505M-12.
[24] Yao H, Tan Z, He D, Zhou Z, Xue Y, Chui L, et al. High strength and ductility AlCrFeNiV high entropy alloy with hierarchically heterogeneous microstructure prepared by selective laser melting. Journal of Alloys and Compounds. 2020; 813: 152196.
[25] Fu N, Tang X, Li D.Y, Parent L, Tian H. In situ investigation of local corrosion at interphase boundary under an electrochemical-atomic force microscope. Journal of Solid-State Electrochemistry. 2015, 19: 337-344.
[26] Šatovic D, Zulj L.V, Desnica V, Fazinic S, Martinez S. Corrosion evaluation and surface characterization of the corrosion product layer formed on Cu–6Sn bronze in aqueous Na2SO4 solution. Corrosion Science. 2009; 51(8): 1596-1603.
[27] Zeng C, Zhang B, Hemmasian A, Wen H, Yao H, Meng W.J, et al. Mechanical, thermal, and corrosion properties of Cu-10Sn alloy prepared by laser-powder-bed-fusion additive manufacturing. Additive Manufacturing. 2020; 35(7): 101411.